

# ANISOTROPY OF THE ROUGH TURBULENT BOUNDARY LAYER SUBJECT TO A FAVORABLE PRESSURE GRADIENT

**Raúl Bayoán Cal**

Department of Mechanical Engineering,  
The Johns Hopkins University,  
3400 N. Charles St., Baltimore, Maryland 21218, USA  
bayoan.cal@jhu.edu

**Brian Brzek & Luciano Castillo**

Department of Mechanical, Aeronautical and Nuclear Engineering,  
Rensselaer Polytechnic Institute,  
110 8th st. Troy, New York 12180, USA

**Gunnar Johansson**

Department of Applied Mechanics,  
Chalmers University of Technology,  
Hörsalsvägen 7, SE-412 96 Göteborg, Sweden

## ABSTRACT

Laser-Doppler anemometry (LDA) measurements of the mean velocity and Reynolds stresses are carried out on a rough surface favorable pressure gradient (FPG) turbulent boundary layer. These data are compared with smooth FPG turbulent boundary layer data possessing the same strength of pressure gradient and with rough zero pressure gradient (ZPG) data. In order to properly capture the  $x$ -dependence of the single point statistics, consecutive measurements of 11 streamwise locations were performed. It is observed through the anisotropy coefficients that the isotropy of the flow is promoted by both the rough surface and the pressure gradient. The isotropization of the boundary layer close to the wall is increased by the roughness, while on the outer part of the boundary layer it is caused by the favorable pressure gradient imposed on the flow. It is also shown through the production terms that the roughness causes a greater production of the turbulence on the outer flow.

## INTRODUCTION

The effects of roughness and favorable pressure gradient on turbulent boundary layers have been studied extensively, but separately. The relationship and influence of these effects occurring simultaneously on the turbulent boundary layer have been once reported by Coleman *et al.* (1977), where hot-wire anemometry was used to measure the velocity field in three downstream locations in a turbulent boundary layer subject to both roughness and FPGs. The roughness used was an arrangement of copper spheres and the external favorable pressure gradient was created using a flexible Plexiglass upper wall. The study focused primarily on equilibrium conditions of these flows as proposed by Clauser (1954). The skin friction was acquired using the momentum integral equation without the inclusion of the  $\langle u^2 \rangle$  and  $\langle v^2 \rangle$  terms. A pressure gradient parameter for rough wall was also suggested as,  $K_r = r/U_\infty dU_\infty/dx$ , where  $r$  is the radius of the spheres. A variety of velocity scales and length scales were used to normalize the profiles.

Unfortunately, these measurements lacked adequate near-wall resolution, especially for the Reynolds stresses. Up to date, this study is the only one which combines these two effects.

Rough surfaces were initially studied by Nikuradse (1950) on pipe flows and different roughness regimes were defined. The regimes were based on the non-dimensional parameter which contains the equivalent sand grain roughness,  $k_{eq}$ , given as  $k^+ = k_{eq}u_*/\nu$ , where  $u_*$  is the friction velocity and  $\nu$  is the kinematic viscosity. Rough turbulent boundary layers were classified as hydraulically smooth (i.e.,  $k^+ < 5$ ), transitionally rough (i.e.,  $5 < k^+ < 70$ ) and fully rough ( $k^+ > 70$ ). Favorable pressure gradients are characterized by an acceleration parameter given as,  $K = \nu/U_\infty^2 dU_\infty/dx$ . FPG flows were first studied by Ludweig and Tillman (1950) and Kline *et al.* (1967).

In rough ZPG turbulent boundary layers, analysis of the anisotropy of the flow has been used with the purpose of understanding the influence of the surface roughness on the turbulence structures. Several studies have observed how this parameter is affected due to roughness, such as those by Antonia *et al.* (1994), Smalley *et al.* (2002) and Keirsbulck *et al.* (2002) on ZPG flows. The major observation is the decrease of the anisotropy in the wall region. The anisotropy tensor is defined as  $b_{ij} = \overline{u_i u_j} / 2k - \delta_{ij} / 3$ , where  $k = 1/2 \overline{u_i u_i}$  is the average turbulent kinetic energy (Choi and Lumley, 2001). In these studies, the anisotropy tensor along with the invariants of the flow were used. The purpose of these invariant techniques is to characterize the structure and organization of the flow. Smalley *et al.* (2002) applied these techniques to zero pressure gradient turbulent boundary layers. Fernholz and Warnack (1998) investigated the anisotropy of a smooth wall favorable pressure gradient turbulent boundary layer through the ratio of the Reynolds stresses,  $(\langle u^2 \rangle / \langle v^2 \rangle)^{1/2}$ , but results for rough FPG flows have yet to be reported.

The effects of roughness and favorable pressure gradients have yet to be reported in the literature especially in regard to near-wall measurements and Reynolds stresses. There-

fore, LDA measurements of a rough turbulent boundary layer, subject to a favorable pressure gradient are reported here to provide further insight on the interaction between the pressure gradient and the surface roughness, particularly their role in the near-wall region. A unique feature of this experiment is the 11 consecutive streamwise locations, where the flow field was measured, which yielded both a total of 33 profiles and accurate methods of the skin friction. Therefore, the x-dependence of the flow is known, and thus gradients of the streamwise component could be calculated (i.e., production,  $dU/dx$ ,  $\tau_w/\rho$ , etc.).

## EXPERIMENTAL SETUP

The wind-tunnel facility used for these current experiments is the L2 wind-tunnel at the Department of Applied Mechanics at Chalmers University of Technology. The facility is a conventional closed-loop design, equipped with turning vanes in all four corners with honeycombs and screens. The contraction ratio is 5.6:1, and the free-stream turbulence level is 0.1%. The test section is 3 m long, 1.8 m wide and 1.25 m high. A specially manufactured aluminum plate is mounted vertically at an angle,  $\alpha$  as seen in figure 1. The plate has dimensions of 2.5 m long, 1.25 m wide, and 5 mm thick. The nose of the plate is placed 200 mm downstream from the test section entrance. In both the smooth and rough FPG experiments, the plate is kept at an angle of 15 degrees to the incoming air stream. Measurements are performed in 11 downstream locations, moving from 1.30 m up to 2.30 m from the leading edge of the plate. In the ZPG case, the local free-stream speed is of course constant equal to  $U_o$ . In the FPG cases, the local free-stream speed increases, and reaches 13 m/s at the first measuring station and 19 m/s at the last one. The error in the Reynolds stress measurements is estimated to be about 1.5%, while the error in the mean velocity measurements is less than 1%. The closest measurements for the rough surface is made at about  $y^+ \approx 25$ . Details about the LDA system may be found in Cal *et al.* (2006).

Each experiment isolates the effect of each external condition to observe its influence on the downstream flow. Three of the upstream conditions are fixed and are the same for all three cases considered: (1) the upstream wind-tunnel speed,  $U_o$ , (2) trip-wire size,  $d_o$ , and (3) trip-wire location,  $x_o$  and shown in figure 1. These conditions have values of 10 m/s, 2 mm and 150 mm, respectively. Table 1 shows the case number in the first column. The second column from the left hand side, corresponds to the angle of the plate,  $\alpha$ , which determines the strength of the pressure gradient. Next, the physical surface is tabulated. The next column denotes the roughness parameter,  $k^+$ , range, which includes all three regimes: hydraulically smooth, transitional, and fully rough. Also, the  $\bar{k}$  ranges for the different cases are

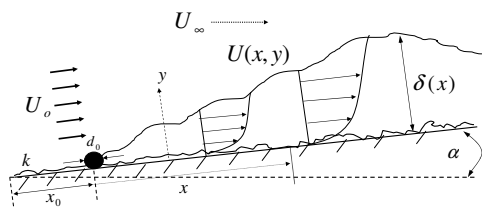


Figure 1: Depiction of the rough turbulent boundary layer subject to a favorable pressure gradient.

Table 1: External conditions for the experimental turbulent boundary layers.

Case	$\alpha$ (deg)	surface	$k^+$	$\bar{k}$
1	15	smooth	0	0
2	15	24-grit	83 - 141	0.087 - 0.099
3	0	24-grit	49 - 54	0.035 - 0.053

shown where  $\bar{k} = k/\delta$  is the variable stipulated by Jiménez (2004) to satisfy the Townsend (1976) similarity hypothesis, which consists of the equality of the rough and smooth velocity profiles in the outer flow. The hypothesis is satisfied for values of this parameter lower than 0.02 at high Reynolds numbers; while for greater values of  $\bar{k}$ , there is a breakdown of the hypothesis, where on the outer layer there is an influence due to the roughness. In table 2, the dependent variables are shown. The Reynolds numbers,  $Re_\theta$  and  $\delta^+$ , are represented in the next two columns. Finally, the range for the skin friction,  $C_f$ , values is shown in the last column. These three quantities are dependent variables and should not be considered as external or upstream conditions.

Table 2: Dependent variables for the experimental turbulent boundary layers.

Case	$Re_\theta$	$\delta^+$	$C_f \times 10^{-3}$
1	1118 - 1552	389 - 589	3.71 - 4.51
2	2066 - 3399	837 - 1620	8.40 - 10.30
3	3309 - 4927	1040 - 1440	4.84 - 5.72

The rough surface considered in these experiments is a 24-grit, aluminum oxide open coated sandpaper. The sheet is attached to the entire length of the aluminum plate and wrapped around the leading edge. The sheet is 0.6 m wide, and is placed in the center of the 1.25 m high plate. Double-sided tape covering the majority of the surface is used to attach the sandpaper to the aluminum plate. The roughness height,  $k$ , used in this investigation is the average of the 5 highest peaks and 5 deepest valleys. The friction velocity is obtained through the integrated momentum integral equation. The error in the skin friction is about 5%.

## RESULTS

The whole velocity field is measured, including the mean velocity and the Reynolds stresses for 11 consecutive streamwise locations. In the present study, the Reynolds stress components are presented. The anisotropy tensor and production terms are also investigated in order to extract the influence of the strong external pressure gradient on a rough wall FPG turbulent boundary layer.

### The Reynolds Stress Profiles

The Reynolds stress components,  $\langle u^2 \rangle$ ,  $\langle v^2 \rangle$  and  $\langle uv \rangle$  are normalized using the friction velocity,  $u_*^2$ , and the free-stream velocity,  $U_\infty^2$ , as will be appreciated in figures 2 through 7. Starting with the streamwise normal component of the Reynolds stress tensor, the friction velocity is employed to normalize the profiles in figure 2. Here the effects of roughness are masked since the effects due to the surface roughness are nearly removed, but the effects produced by the favorable pressure gradient are observed where

the magnitude of  $\langle u^2 \rangle$  diminishes due to the FPG. There is also a Reynolds number dependence on the profiles subject to a FPG. The scaling removes the effects of roughness from the outer flow, but does not remove effects induced by the favorable pressure gradient. Notice that close to the wall ( $\bar{y} \leq 0.1$ ),  $\langle u^2 \rangle$  is flat for the rough data while the smooth data still continues to increase.

When using the free-stream velocity, the profiles show the effects of the rough wall and a slight difference exists on the outer layer due to the FPG as observed in figure 3. The effect of roughness dominates the boundary layer when comparing the magnitude of its influence on the profiles. The magnitude of the stress is higher for the rough surface than for the smooth surface everywhere except very close to the wall. This indicates that there is a higher influence of the roughness than the pressure gradient on the outer flow. Furthermore, the profiles tend to increase, near the wall as a result of the combined action of roughness and pressure gradient. Very close to the wall, the effect of roughness destroys the viscous sublayer region. Consequently, the near-wall peak in  $\langle u^2 \rangle$  is diminished which produces a flatter profile of  $\langle u^2 \rangle$  regardless of the scaling ( $U_\infty^2$  or  $u_*^2$ ). Conversely, the profiles show a moderate difference due to the strength of the pressure gradient for this particular component in the outer region. Although a slight increase in magnitude is noticed close to the wall, the pressure slightly damps the fluctuations in the outer part of the boundary layers regardless of the scaling although it is more evident with  $u_*^2$ . The high peak close to the wall and damping away from the wall are due to the pressure diffusion term  $\langle pv \rangle$  and balance of the pressure on the  $y$  momentum equation, respectively. This argument gives further indication that the roughness effects supersede those caused by the pressure gradient. The shape of the profiles are also different for smooth to rough surfaces over the entire boundary layer, as shown in figure 3. This observation is demonstrated in the inner region as seen on the insert graph of figure 3, which is plotted in semi-log scale. A deduced observation is that the increase in strength of the pressure gradient leads to a lower value of the Reynolds stress. However, the effect of roughness counteracts the effect of the favorable pressure gradient. Noticing the profiles in semi-log scale, the change in shape over the entire inner and outer regions is evident.

The wall-normal component  $\langle v^2 \rangle$  of the Reynolds

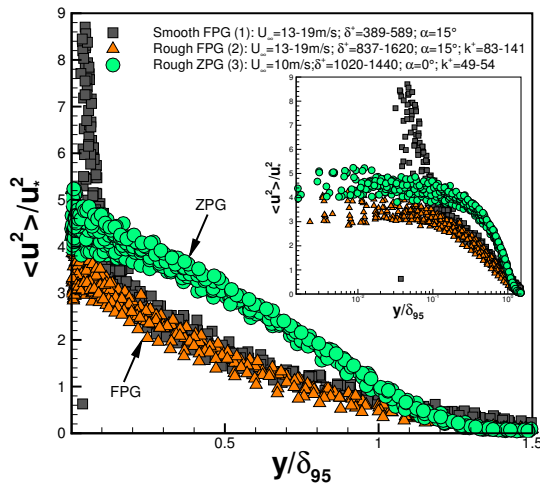


Figure 2: Reynolds normal stress,  $\langle u^2 \rangle$ , profiles normalized with  $u_*^2$ .

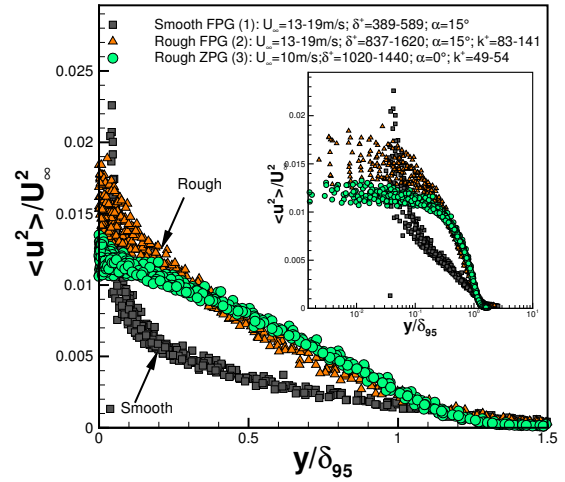


Figure 3: Reynolds normal stress,  $\langle u^2 \rangle$ , profiles normalized with  $U_\infty^2$ .

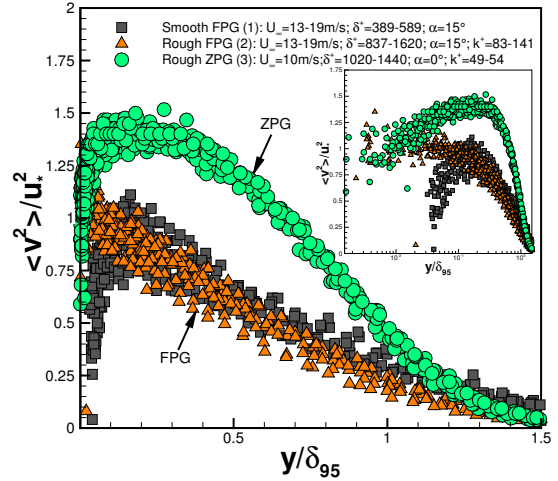


Figure 4: Reynolds normal stress,  $\langle v^2 \rangle$ , profiles normalized with  $u_*^2$ .

stress tensor shows the influence of the external conditions present (surface roughness and strength of the pressure gradient) as seen in figures 4 and 5. The profiles normalized with the friction velocity exhibit not only a Reynolds number dependence for the FPG data but also there is not much difference between the rough data (sets 2 and 3) in figure 4. The difference exists in the shape of the profiles where close to the wall the roughness causes a slight upward shift on the data. However, an increase in the favorable pressure gradient condition causes a decrease in this component of the Reynolds stress on the outer flow when scaled with  $u_*^2$  or  $U_\infty^2$  (figs. 4 and 5). When scaled with the free-stream velocity, both effects are evident here, contrary to the observations on the streamwise component of the Reynolds stresses. In figure 5, the behavior of this component changes when comparing the ZPG and FPG flows on a rough wall. The rough FPG data is damped away from the wall ( $\bar{y} \approx 0.5$ ) faster than the rough ZPG data. Furthermore, the shape of the profiles is nearly the same in the outer layer for the smooth and rough wall FPG boundary layers, as seen in figure 5 despite the large difference in magnitude. The profiles change close to the wall, where the FPG augments the magnitude of the stress. This component exhibits the largest difference

in magnitude due to a favorable pressure compared to the  $\langle u^2 \rangle$  and  $\langle uv \rangle$  components. Also, it is notable that the set of data does not show a significant Reynolds number dependence. In addition, the external FPG alters the outer region of the  $\langle v^2 \rangle$  component. This is in agreement with the study of Castillo *et al.* (2006) for smooth FPG flows approaching quasi-laminarization.

In figures 6 and 7, the Reynolds shear stress,  $\langle uv \rangle$ , is normalized by  $u_*^2$  and  $U_\infty^2$ . In figure 6, the data normalized with the friction velocity exhibits a similar trend as in the  $\langle v^2 \rangle$  component where the major difference is observed when the rough data sets are compared (sets 2 & 3). There is a decrease in the profiles due to the imposed pressure gradient condition in the outer region. When using  $U_\infty^2$ , the same trends as in the wall-normal component are apparent. The Reynolds shear stress shows a large shift upwards on the profiles due to the surface roughness as appreciated from figure 7, especially near the wall. The effects of the pressure gradient are again noticeable, where close to the wall, the rough FPG data displaces upwards in comparison to the rough ZPG data. Furthermore, it is observed that all of the Reynolds stresses are Reynolds number,  $\delta^+$ , independent within the (rather small) Reynolds number intervals investigated here. The equivalent values in  $Re_\theta$  is 1118 to about 4927. It is in this range of Reynolds number where the greatest variation due to Reynolds number exists in the boundary layer. It is evident that the sand grain roughness alters the shape of profiles in the inner region by increasing the magnitude of the component all along the boundary layer.

### The Anisotropy Tensor

In order to investigate the possibility that a rough surface and a favorable pressure gradient promote isotropy, the anisotropy tensor is herein investigated. The anisotropy tensor,  $b_{ij} = \overline{u_i u_j} / 2k - \delta_{ij} / 3$ , is computed using the different components of the Reynolds stress. For the calculation of  $b_{ij}$ , the kinetic energy used to normalize the stresses does not contain the third component of the Reynolds normal stress,  $\langle w^2 \rangle$ , since only 2-D measurements of the velocity field are performed.

Figures 8 through 10 show the different components of the anisotropy tensor. The overall result is that the flow be-

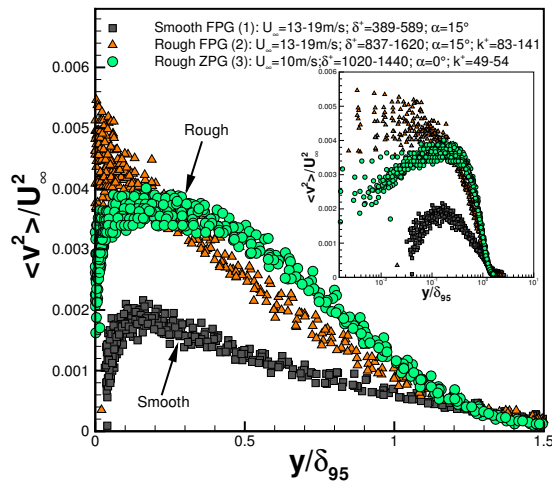


Figure 5: Reynolds normal stress,  $\langle v^2 \rangle$ , profiles normalized with  $U_\infty^2$ .

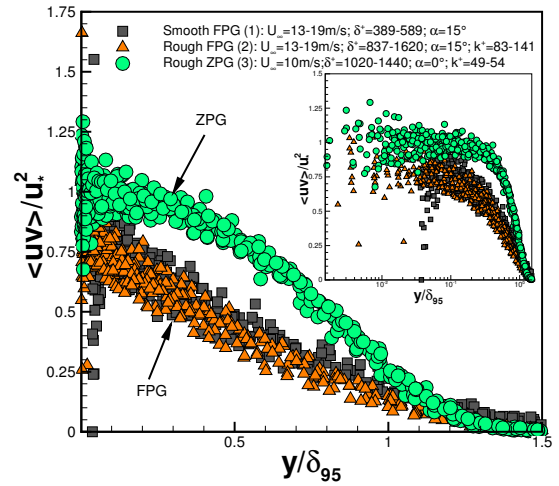


Figure 6: Reynolds shear stress,  $\langle uv \rangle$ , profiles normalized with  $u_*^2$ .

comes more isotropic due to the roughness at the wall. The contrary is concluded for the favorable pressure gradient, depending on the considered component. As previously noted, the  $\langle u^2 \rangle$  component is the Reynolds stress component that suffers the most changes in shape due to the surface roughness. This is now explained through the streamwise component of the anisotropy tensor,  $b_{11}$ , as viewed in figure 8. It is observed that the anisotropy close to the wall is directly affected by the rough wall, and is decreased as seen in the semi-log plot. These changes occur mainly from  $\bar{y} < 0.1$ . Furthermore, the anisotropy is larger in the outer part of the boundary layer for the case with a favorable pressure gradient. This observation is evident given that in order to obtain an isotropic flow,  $b_{ij}$  equals zero as pointed by Smalley *et al.* (2002). These effects are viewed past  $\bar{y} > 1$ , well into the outer layer. Consequently, the surface roughness promotes isotropy on the inner flow while the FPG produces the inverse effect, but on the outer flow.

Figure 9 is the shear component of the anisotropy tensor,  $-b_{12}$ . There is a difference in the behavior of this component compared with the previous one. Only the inner part of the component is affected; again showing its effects below

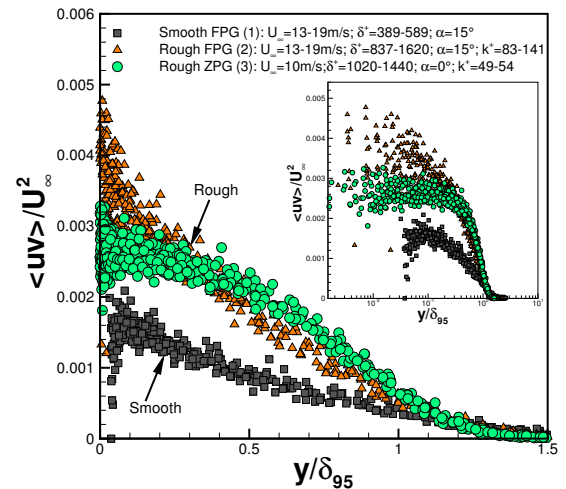


Figure 7: Reynolds normal stress,  $\langle uv \rangle$ , profiles normalized with  $U_\infty^2$ .

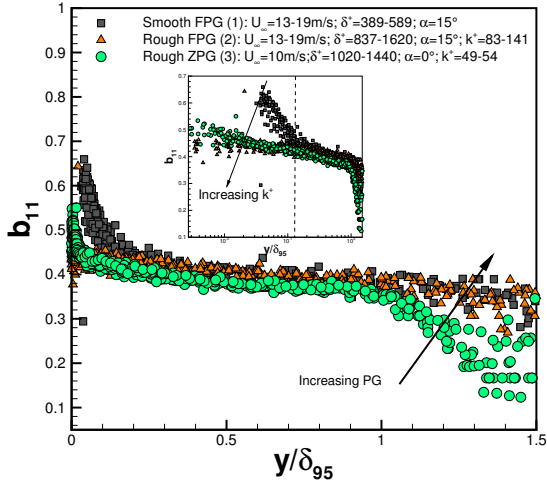


Figure 8: Anisotropy component  $b_{11}$ .

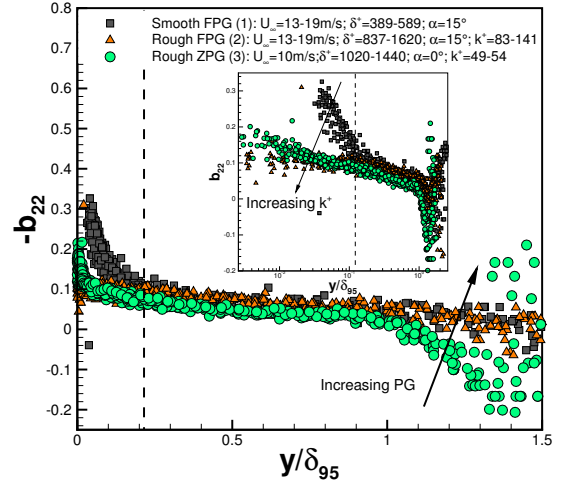


Figure 10: Anisotropy component  $b_{22}$ .

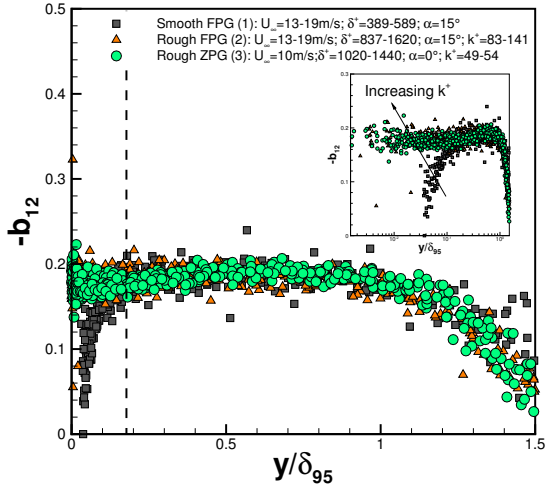


Figure 9: Anisotropy component  $b_{12}$ .

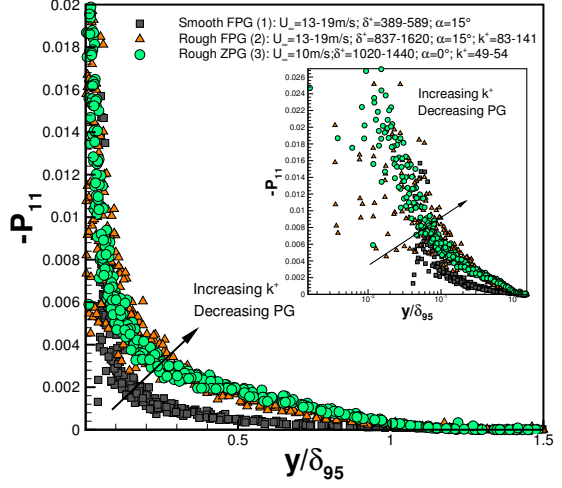


Figure 11: Production component,  $P_{11}$ .

$y/\delta_{95} < 0.1$  as observed in the semi-log scale plot. However, the pressure gradient does not play an important role on this component in the inner or outer flow. In general,  $b_{12}$  is not affected by the pressure gradient but is affected by the roughness only in the inner part. This is the major difference between this component and the previous component. Lastly, the wall-normal component of the anisotropy tensor,  $-b_{22}$ , is shown in figure 10. The behavior of this component is quite different than that of the  $b_{11}$ . The thresholds of this parameter are exactly the same as in the  $b_{11}$  due to the influence of the favorable pressure gradient and rough surface on the boundary layer. The difference in this component is that the favorable pressure gradient effect decreases the anisotropy away from the wall where  $-b_{22}$  is almost zero. There is a sharp increase in the outer layer for this component as seen past  $y/\delta_{95} > 1.1$  in the case without pressure gradient.

### The Production Term

Given the vast number of consecutive measurements along the plate, the  $x$ -dependence is obtained and the production term is computed. The production term is given by,  $P_{ij} = -\langle u_i u_k \rangle \partial U_j / \partial x_k - \langle u_j u_k \rangle \partial U_i / \partial x_k$ . This quantity is responsible for the production of the Reynolds

stress, due to the mean velocity gradients. The  $P_{11}$  and the  $P_{12}$  components of the production are normalized with  $U_\infty^3 / \delta_{95}$ . It is important to note that the terms which possess the  $x$ -dependence are usually neglected (i.e.,  $\partial U / \partial x$ ,  $\partial V / \partial x$ ) since usually not more than one downstream location is measured. However, the  $x$ -dependence is negligible compared to the wall normal gradients for ZPG flows.

The  $P_{11}$  component of production is shown in figure 11 and it is normalized with  $U_\infty^3 / \delta_{95}$ . The curves for both rough cases fall almost on top of each other, but if observed carefully, in the outer part of the boundary layer the production of the rough ZPG is higher than the rough FPG. As a consequence, this reinforces the point that increasing the FPG suppresses the turbulence production despite the effects of roughness. In terms of the roughness effect, it is easily noticed that the rough surface enhances the turbulence. This is consistent with the observations in the previous sections, (i.e., increase in the Reynolds stresses).

The other computed component of the production term is the production of the Reynolds shear stress,  $P_{12}$ , displays the same behavior as  $P_{11}$  as shown in figure 12. Moreover, the profiles increase marginally in magnitude as the strength of the favorable pressure gradient is decreased. This means that for this component, the roughness enhances the production of the turbulence significantly while the pressure

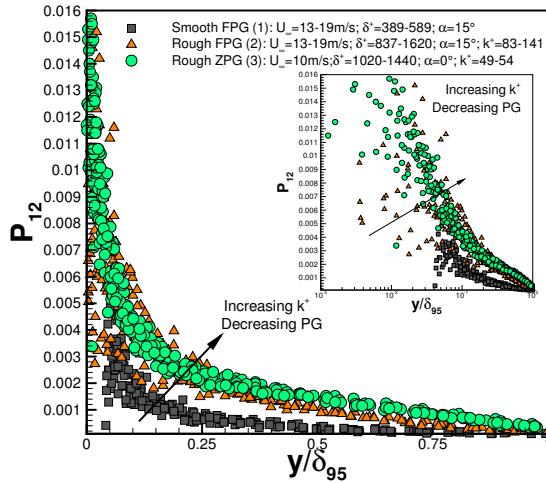


Figure 12: Production component,  $P_{12}$ .

gradient diminishes it. Also, both components  $P_{11}$  and  $P_{12}$  are of the same order of magnitude.

There are no production terms present in the  $\langle v^2 \rangle$  and  $\langle w^2 \rangle$  components of the Reynolds stress equation. This allows for the further conclusion that the production in these two directions (wall-normal and spanwise) is ‘injected’ by the redistribution of energy through the pressure strain terms. Following this statement, the pressure diffusion terms decrease due to two factors: (i) The acceleration created by the favorable pressure gradient, and (ii) the production acts against the pressure strain terms (see the opposite signs of production and pressure strain). The same is deduced for the dissipation of turbulence. This means that the flow becomes less dissipative due to the imposed FPG on the flow. It also damps turbulence on the outer layer while enhancing it close to the wall. On the other hand, the surface roughness enhances the production of turbulence. This acts ‘negatively’ with the pressure strain rate and the opposite with dissipation. The surface roughness then increases the exchange of energy amongst components through the pressure strain rate and also increases the dissipation of the flow. As a consequence, there is a balance between the FPG and the surface roughness. In general, the effect of the surface roughness is higher than the FPG in terms of magnitude.

## CONCLUSIONS

LDA measurements on a 2-D flow are carried out over 11 consecutive streamwise locations for three different experimental conditions yielding 33 profiles. Consequently, the x-dependence of the boundary layer is reported in this study are used to obtain the wall shear stress and production terms. This is the first experiment with near-wall measurements using LDA on rough FPG turbulent boundary layers. The shape of the streamwise component of the Reynolds stress changes entirely in the inner region due to the roughness imposed at the wall and the strength of the pressure gradient. Furthermore, although there is an increase in the magnitude of  $\langle v^2 \rangle$  component, the shape for the rough FPG resembles that of the smooth ZPG data. The profiles also become flatter due to the influence of the roughness parameter close to the wall thus destroying coherent structures created in the inner layer. The same is observed for the  $\langle u^2 \rangle$  and  $\langle uv \rangle$  components, but the pressure gradient condition is not as evident on these components as on

the  $\langle v^2 \rangle$  component. The friction velocity scaling is more susceptible to the pressure gradient condition rather than the surface roughness while the free-stream velocity shows the reverse observation.

Furthermore, as shown through the anisotropy tensor, the flow becomes more isotropic due to the effects of the roughness in the wall region ( $\bar{y} < 0.1$ ). In terms of the favorable pressure gradient, the flow might become either more isotropic or anisotropic depending on which component is analyzed. In the  $b_{22}$  component, the flow becomes more isotropic due to the FPG on the outer part of the boundary layer. In the  $b_{11}$  component, the effects of the FPG are to cause anisotropy on the flow. The  $b_{12}$  component is not affected by external favorable pressure gradient imposed on the outer flow. In addition, the production of turbulence is suppressed due to the FPG in the outer part of the boundary layer. Inversely, the surface roughness tends to induce turbulence close to the wall.

## REFERENCES

- Antonia, R. A., Djenidi, L., and Spalart, P. R., 1994, “Anisotropy of the dissipation tensor in a turbulent boundary layer”, *Phys. of Fluids*, Vol. 6, (7), pp. 2475-2479.
- Cal, R. B., Johansson, G., and Castillo, L. 2006, “Upstream condition effects on turbulent boundary layers subject to favorable pressure gradients”, *AIAA J.*, Vol. 44, 11, pp. 2488-2499.
- Castillo, L., Cal, R. B., and Johansson, T. G., 2006, “Evolution of the favorable pressure gradient turbulent boundary layer towards a quasi-laminar state,” (invited) *AIAA-2006-2883*, 36th AIAA Fluid Dynamics Conference and Exhibit, San Francisco, CA, June 5-8.
- Clauser, F. H., 1954, “Turbulent boundary layers in adverse pressure gradients”, *J. Aero. Sci.*, Vol. 21, pp. 91-108.
- Choi, K.-S., and Lumley, J. L., 2001, “The return to isotropy of homogeneous turbulence”, *J. Fluid Mech.*, Vol. 436, pp. 59-84.
- Coleman, H. W., Moffat, R. J., and Kays, W. M., 1977, “The accelerated fully rough turbulent boundary layer”, *J. Fluid Mech.*, Vol. 82, pp. 507-528.
- Fernholz, H. H., and Warnack, D., 1998, “The effects of a favorable pressure gradient and of the Reynolds number on an incompressible axisymmetric turbulent boundary layer. Part 1. The turbulent boundary layer”, *J. Fluid Mech.*, Vol. 359, pp. 329-356.
- Jiménez, J. 2004, “Turbulent flows over rough walls”, *Annu. Rev. Fluid Mech.*, Vol. 36, pp. 173-196.
- Keirsbulck, L., Labraga, L., Mazouz, A., and Tournier, C., 2002, “Influence of surface roughness on anisotropy in a turbulent boundary layer flow”, *Experiments in Fluids*, Vol. 33, pp. 497-499.
- Kline, S. J., Reynolds, W. C., Schraub, F. A., and Runstadler, P. W., 1967, “The structure of turbulent boundary layers”, *J. Fluid Mech.*, Vol. 30, pp. 741-773.
- Ludwig, H., and Tillman, W., 1950, “Investigations of the wall shearing stress in turbulent boundary layers.” *NACA TM 1285*.
- Nikuradse, J., 1950, “Laws of flows in rough pipes”, *NACA TM 1292*.
- Smalley, R. J., Leonardi, S., Antonia, R. A., Djenidi, L., and Orlandi, P., 2002, “Reynolds stress anisotropy of turbulent rough wall layers,” *Experiments in Fluids*, Vol. 33, pp. 31-37.
- Townsend, A. A., 1976, “The structure of turbulent shear flow”, Cambridge University Press, pp. 150-158.